Similarities and Differences between Phenoxyl and Tyrosine Phenoxyl Radical Structures, Vibrational Frequencies, and Spin Densities

Yue Qin and Ralph A. Wheeler*

Contribution from the Department of Chemistry and Biochemistry, University of Oklahoma, 620 Parrington Oval, Room 208, Norman, Oklahoma 73019

Received November 3, 1994[⊗]

Abstract: Tyrosine phenoxyl radical (TyrO•) has been detected recently in a number of proteins by comparing experimentally observed electron paramagnetic resonance, UV resonance Raman, or Fourier transform IR vibrational spectra with the corresponding spectra for the organic phenoxyl radical (PhO•). Density-functional calculations are described to illustrate the strengths and limitations of the phenoxyl radical model for the structures, electronic spin densities, vibrational frequencies, and vibrational modes of TyrO•. Both the PhO• and TyrO• radicals display substantial C=O double bond character, whereas distances within the carbon ring are intermediate between distances observed for the corresponding bonds of phenol and *p*-benzoquinone. The striking structural similarity between the two radicals appears despite the proximity of the CO_2H and NH_2 groups located gauche to the phenoxyl side chain of TyrO• in the amino acid radical's most stable calculated gas-phase conformation. Electronic spin densities calculated for the atoms of both PhO• and TyrO• agree well with experimentally derived spin density ratios and display a pattern characteristic of odd-alternant hydrocarbons. Calculated spin densities for the two radicals differ from each other by less than 0.03, implying that the unpaired electron of TyrO• resides entirely on its phenoxyl side chain. Calculated, harmonic vibrational frequencies for both PhO• and TyrO• are within −3.3% to +3.9% of experimentally determined frequencies. Most vibrational frequencies and modes involving motions within the ring planes of PhO• and TyrO• are also very similar to each other. The largest frequency shifts upon replacing the hydrogen of PhO• with the peptide chain of TyrO• can be attributed to two effects: (1) the different bonding and mass of the peptide chain compared to the hydrogen it replaces in PhO• and (2) interactions between the TyrO• peptide chain and its phenoxyl side chain. TyrO• modes with the largest mixing between peptide chain and phenoxyl side chain motions are identified, as they are likely to be most sensitive to TyrO• conformation and offer the best potential for studying subtle conformational differences between TyrO• radicals in different proteins. Calculated isotopic frequency shifts for TyrO•-d_7 and TyrO•-$^{13}C_6$ are also reported to aid in mode assignments. Furthermore, the $C^{\zeta}O^{\eta}$ stretching mode is the only mode of TyrO•-$^{18}O^{\eta}$ and TyrO•-$^{13}C^{\zeta}$ calculated to appear above 1350 cm^{-1} that displays a substantial isotopic frequency shift (−24 and −37 cm^{-1}, respectively). Thus, the $C^{\zeta}O^{\eta}$ stretching mode may be identified by either $^{18}O^{\eta}$ or $^{13}C^{\zeta}$ isotopic substitution experiment.

Introduction

Amino acid radicals are implicated in cancer, aging, and a number of productive biochemical reactions.[1−3] For example, tyrosine phenoxyl radical (TyrO•; one gas-phase resonance form is shown in **1**) has been detected recently in a number of

1

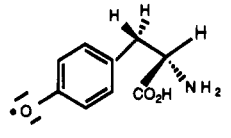

TyrO•

proteins[1−4] including ribonucleotide reductase,[5−9] prostaglandin H synthase,[10−12] and the photosynthetic reaction center of the oxygen-evolving photosystem II.[13−15] Covalently modified analogues of TyrO• have also been detected in galactose oxidase[16,17] and amine oxidases.[18] Although the biological function of these radicals is not always clear, they are known to form covalent cross-links between DNA and proteins,[19]

[⊗] Abstract published in *Advance ACS Abstracts*, May 15, 1995.

(1) *Metal Ions in Biological Systems, Volume 30: Metalloenzymes Involving Amino-Acid Residue and Related Radicals*; Sigel, H., Sigel, A., Eds.; Marcel Dekker: New York, 1994.
(2) Stubbe, J. A. *Annu. Rev. Biochem.* **1989**, *58*, 257−285.
(3) Pedersen, J. Z.; Finazzi-Agró, A. F. *FEBS Lett.* **1993**, *325*, 53−58.
(4) Prince, R. C. *Trends Biochem. Sci.* **1988**, *13*, 286−288.
(5) Norlund, P.; Sjöberg, B.-M.; Eklund, H. *Nature* **1990**, *345*, 593−598.
(6) Bender, C. J.; Sahlin, M.; Babcock, G. T.; Barry, B. A.; Chandrashekar, T. K.; Salowe, S. P.; Stubbe, J.; Lindström, B.; Petersson, L.; Ehrenberg, A.; Sjöberg, B.-M. *J. Am. Chem. Soc.* **1989**, *111*, 8076−8038.
(7) Backes, G.; Sahlin, M.; Sjöberg, B.-M.; Loehr, T. M.; Sanders-Loehr, J. *Biochemistry* **1989**, *28*, 1923−1929.
(8) Sjöberg, B.-M.; Gräslund, A. *Adv. Inorg. Biochem.* **1983**, *5*, 87−110.
(9) Sjöberg, B.-M.; Reichard, P.; Graslund, A.; Ehrenberg, A. *J. Biol. Chem.* **1978**, *253*, 6863−6865.
(10) Tsai, A.; Hsi, L. C.; Kulmacz, R. J.; Palmer, G.; Smith, W. L. *J. Biol. Chem.* **1994**, *269*, 5085−5091.
(11) Smith, W. L.; Eling, T. E.; Kulmacz, R. J.; Marnett, L. J.; Tsai, A. L. *Biochemistry* **1992**, *31*, 3−7.
(12) DeGray, J. A.; Lassmann, G.; Curtis, J. F.; Kennedy, T. A.; Marnett, L. J.; Eling, T. E.; Mason, R. P. *J. Biol. Chem.* **1992**, *267*, 23583−23588.
(13) Hoganson, C. W.; Babcock, G. T. In *Metal Ions in Biological Systems, Volume 30: Metalloenzymes Involving Amino-Acid and Related Radicals*; Sigel, H., Sigel, A., Eds.; Marcel Dekker: New York, 1994; pp 77−107.
(14) Babcock, G. T. *Proc. Natl. Acad. Sci. U.S.A.* **1993**, *90*, 10893−10895.
(15) Barry, B. A. *Photochem. Photobiol.* **1993**, *57*, 179−188.
(16) Babcock, G. T.; El-Deeb, M. K.; Sandusky, P. O.; Whittaker, M. M.; Whittaker, J. W. *J. Am. Chem. Soc.* **1992**, *114*, 3727−3734.
(17) Whittaker, M. M.; Whittaker, J. W. *J. Biol. Chem.* **1990**, *265*, 9610−9613.

0002-7863/95/1517-6083$09.00/0

catalyze a number of biosynthetic reactions,[5,8,11,17,18] and serve as an electron transfer intermediate in photosynthesis.[13-15] Intense efforts are also underway to prepare and characterize model compounds with the same spectral features and ultimately the same chemical properties as proteins containing TyrO•.[20]

To identify and characterize the TyrO•-containing amino acid residues found in different proteins, a number of clever experiments have been carried out to combine isotopic substitution or site-directed mutagenesis with electron paramagnetic resonance (EPR), electron-nuclear double resonance (ENDOR), or vibrational spectroscopic measurements.[10,21-26] These workers typically compare measured EPR or ENDOR spectra for the suspected TyrO•-containing proteins with corresponding spectra for the organic phenoxyl radical (PhO•, see **2**), its

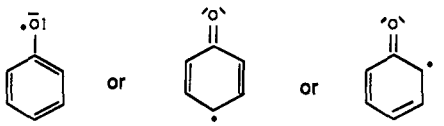

2

p-methyl derivative (*p*-cresol), or *in vitro* TyrO•. More recently, significant advances in ultraviolet resonance Raman[27,28] and difference Fourier transform infrared[29] vibrational spectroscopies have allowed a similar comparison of TyrO• vibrational spectra in proteins with those for the simpler model structures.[7,30-32] While the analogies between the tyrosine phenoxyl radical side chain and phenoxyl or *p*-cresol radicals are undoubtedly very useful, the limitations of these comparisons remain obscure. Complications inherent in matching the spectral properties of TyrO• and PhO• include the following: (1) different spin density distributions were measured for TyrO• in a number of proteins,[6,33-35] (2) only a limited number of PhO• vibrational frequencies are experimentally observable,[30,36-38] and (3) vibrational spectra for TyrO• in proteins are only beginning to emerge.[7,31,32] This contribution seeks to clarify the strengths and limitations of comparing the physical properties of TyrO• with those of the organic phenoxyl radical by providing calculated structures, spin densities, and harmonic vibrational frequencies and mode assignments for both TyrO• and PhO•. We will therefore describe our density-functional (DF) quantum chemical methods, present calculated results, and compare and contrast the calculated structures, electronic spin density distributions, harmonic vibrational frequencies, and vibrational modes of PhO• with those of the TyrO• side chain. But first, we summarize the currently available EPR, ENDOR, and vibrational spectroscopic data for TyrO• and PhO•.

Experimental Data for Phenoxyl and Tyrosine Phenoxyl Radicals

To our knowledge, experimental bond lengths and angles are currently unavailable for both PhO• and TyrO•, but a variety of spectroscopic data has been reported. Table 1 compares spin densities for TyrO•, inferred from EPR or ENDOR spectroscopic data for a variety of proteins.[6,33-35] Although hydrogen bonding to the phenoxyl oxygen of TyrO• may alter measured spin densities in proteins other than *E. coli* ribonucleotide reductase (*E. coli* RR),[5-7] all EPR/ENDOR measurements agree that the TyrO• side chain has a spin density distribution appropriate for an odd-alternant, cyclic polyene.[39] In *E. coli* RR, for example, TyrO• has nearly zero spin density on both the oxygen-bearing carbon, C^{ζ}, and the carbon located *meta* to C^{ζ}, C^{δ} (throughout this work, we have adopted the atom designations for tyrosine shown in **3** and recommended by the IUPAC-IUB Commission

3

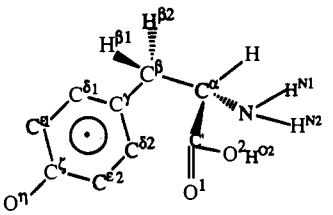

on Biochemical Nomenclature[40] for both PhO• and TyrO•). The largest spin density for TyrO• (0.49) resides on the *para*-carbon atom, C^{γ}, whereas the *ortho*-carbon, C^{ϵ}, carries the second-largest spin density (0.26). Similarly, the phenoxyl oxygen of TyrO• from *E. coli* RR displays a relatively large spin density of 0.16. Spin densities for TyrO• in mouse RR are similar to those measured in *E. coli*, but computer modeling of the photosynthetic reaction center from photosystem II (PSII) implies hydrogen bonding to O^{η},[41,42] so experimental spin densities for PSII and RR may not be directly comparable. We note, however, that spin density ratios for TyrO• in PSII determined by Rigby et al.[34] are almost identical to experimental spin density ratios for PhO•,[43,44] listed in footnote *a* for Table 1. Consequently, both TyrO• and PhO• display a qualitatively similar pattern of alternating large and small spin densities characteristic of odd-alternant hydrocarbons.

Unfortunately, relatively few vibrational frequencies for phenoxyl and tyrosine phenoxyl radical have been measured experimentally. The available, experimentally measured vibrational frequencies for PhO•[30,36-38] and TyrO•[30] are displayed for comparison in Table 2. The highest frequency mode for PhO•, observed at 1552 cm^{-1}, is a CC stretching mode of A_1 symmetry, whereas the A_1 symmetry CO stretching mode appears immediately below, at 1505 cm^{-1}. Next comes a combined CH bending and CC stretching mode at 1398 cm^{-1}, a B_2 symmetry mode composed of CC stretching and CH bending at 1331 cm^{-1}, and

(18) Janes, S. M.; Mu, D.; Wemmes, D.; Smith, A. J.; Kaus, S.; Maltby, D.; Burlingame, A. L.; Klinman, J. P. *Science* **1990**, *248*, 981-987.
(19) Simic, M. G.; Dizdaroglu, M. *Biochemistry* **1985**, *24*, 233-236.
(20) (a) Goldberg, D. P.; Watton, S. P.; Masschelein, A.; Wimmer, L.; Lippard, S. J. *J. Am. Chem. Soc.* **1993**, *115*, 5346-5347. (b) Goldberg, D. P.; Koulougliotis, D.; Brudvig, G. W.; Lippard, S. J. *J. Am. Chem. Soc.* **1995**, *117*, 3134-3144.
(21) Boerner, R. J.; Barry, B. A. *J. Biol. Chem.* **1993**, *268*, 17151-17154.
(22) Barry, B. A.; Babcock, G. T. *Proc. Natl. Acad. Sci. U.S.A.* **1987**, *84*, 7099-7103.
(23) Vermaas, W. F. J.; Rutherford, A. W.; Hansson, O. *Proc. Natl. Acad. Sci. U.S.A.* **1988**, *85*, 8477-8481.
(24) Debus, R. J.; Barry, B. A.; Babcock, G. T.; McIntosh, L. *Proc. Natl. Acad. Sci. U.S.A.* **1988**, *85*, 427-430.
(25) Debus, R. J.; Barry, B. A.; Sithole, I.; Babcock, G. T.; McIntosh, L. *Biochemistry* **1988**, *27*, 9071-9074.
(26) Metz, J. G.; Nixon, P. J.; Rogner, M.; Brudvig, G. W.; Diner, B. A. *Biochemistry* **1989**, *28*, 6960-6969.
(27) Austin, J. C.; Jordan, T.; Spiro, T. G. In *Biomolecular Spectroscopy, Part A*; Clark, R. J. H., Hester, R. E., Eds.; John Wiley & Sons: New York, 1993; pp 55-121.
(28) Asher, S. A. *Annu. Rev. Phys. Chem.* **1988**, *39*, 537-588.
(29) Mäntele, W. *Trends Biochem. Sci.* **1993**, *18*, 197-199.
(30) Johnson, C. R.; Ludwig, M.; Asher, S. A. *J. Am. Chem. Soc.* **1986**, *108*, 905-912.
(31) MacDonald, G. M.; Barry, B. A. *Biochemistry* **1992**, *31*, 9853-9856.
(32) MacDonald, G. M.; Bixby, K. A.; Barry, B. A. *Proc. Natl. Acad. Sci. U.S.A.* **1993**, *90*, 11024-11028.
(33) Warncke, K.; Babcock, G. T.; McCracken, J. *J. Am. Chem. Soc.* **1994**, *116*, 7332-7340.
(34) Rigby, S. E. J.; Nugent, J. H. A.; O'Malley, P. J. *Biochemistry* **1994**, *33*, 1734-1742.
(35) Hoganson, C. W.; Babcock, G. T. *Biochemistry* **1992**, *31*, 11874-11880.
(36) Tripathi, G. N. R.; Schuler, R. H. *Chem. Phys. Lett.* **1983**, *98*, 594-596.
(37) Tripathi, G. N. R.; Schuler, R. H. *J. Chem. Phys.* **1984**, *81*, 113-121.
(38) Tripathi, G. N. R.; Schuler, R. H. *J. Phys. Chem.* **1988**, *92*, 5129-5133.
(39) Salem, L. *Molecular Orbital Theory of Conjugated Systems*; W. A. Benjamin, Inc.: New York, 1966.
(40) Hoffmann-Osterhof, O. et al. *Biochemistry* **1970**, *9*, 3471-3479.
(41) Svensson, B.; Vass, I.; Cedergren, E.; Styring, S. *EMBO J.* **1990**, *9*, 2051-2059.
(42) Ruffle, S. V.; Donnelly, D.; Blundell, T. L.; Nugent, J. H. A. *Photosynth. Res.* **1992**, *34*, 287-300.
(43) Neta, P.; Fessenden, R. W. *J. Phys. Chem.* **1974**, *78*, 523-529.
(44) Stone, T. J.; Waters, W. A. *J. Chem. Soc.* **1964**, 213-218.

Table 1. Experimentally Derived Spin Densities[a] for the Tyrosine Phenoxyl Radical in Mouse Ribonucleotide Reductase, *E. coli* Ribonucleotide Reductase, and One of Two Tyrosine Phenoxyl Radicals (Y_{D}•) in Photosystem II

	TyrO• model[d]	mouse RR[d]	*E. coli* RR[e]	PSII Y_{D}[f]	PSII Y_{D}[d]	PSII Y_{D}[g]
$\varrho(C^{\gamma})$	0.20−0.44	0.33	0.49	0.4	0.14−0.34	0.37
$\varrho(C^{\delta})$			−0.07	−0.07, −0.08		−0.06
$\varrho(C^{\epsilon})$	0.26	0.25	0.26	0.26, 0.27	0.29	0.25
$\varrho(C^{\zeta})$			−0.03	{0.22}[h]		{0.25}[h]
$\varrho(O^{\eta})$	0.45−0.21	0.34	0.16	{0.22}[h]	0.45−0.25	{0.25}[h]

[a] Measured spin density ratios obtained as ratios of hyperfine coupling constants[b,c] for phenoxyl radical are $\varrho(C^{\gamma})/\varrho(C^{\delta})$ = 5.3, 5.5; $\varrho(C^{\gamma})/\varrho(C^{\epsilon})$ = 1.5. [b] Reference 44. [c] Reference 43. [d] Reference 35. [e] Reference 6. [f] Reference 34. [g] Reference 33. [h] The sum of spin densities on C^{ζ} on O^{η}.

Table 2. Experimentally Measured Vibrational Frequencies for Phenoxyl and Tyrosine Phenoxyl Radicals

sym	approximate description	phenoxyl radical[a]	tyrosine radical[b]
A_1	CC str	1552	1565
A_1	CO str	1505	1510
A_1	CH bend/CC str	(1398)[c]	1402
A_1	CH bend	1157	1160
A_1	CH bend/ring breath	1050	
A_1	CCC trig bend	990	975
A_1	ring breath/CCC bend	840	810
A_1	CCC bend	528	
B_2	CH bend/CC str	(1398)[c]	1402
B_2	CC str/CH bend	1331	

[a] References 37 and 38. [b] Reference 30. [c] The band measured at 1398 cm^{-1} has been assigned to two different modes in refs 36 and 38.

a CH bend at 1157 cm^{-1}. Modes involving in-plane breathing or bending of the carbon framework appear next. The band observed at 1050 cm^{-1} was assigned to CH bending plus ring breathing motions; the mode at 990 cm^{-1} involves CCC trigonal bending; and the 840 cm^{-1} mode was described as a mixture of ring breathing and CCC bending. The lowest frequency mode detected experimentally, at 528 cm^{-1} for PhO•, was attributed to a CCC bending mode.

The experimentally determined frequencies for the TyrO• radical appear near those observed for PhO• and have been attributed to very similar modes. For example, the highest frequency mode observed for TyrO• is the CC stretching mode at 1565 cm^{-1}, only 13 cm^{-1} higher in frequency than the corresponding mode for PhO•. The CO stretch at 1510 cm^{-1} is 5 cm^{-1} higher that the phenoxyl CO stretch; the CH bending plus CC stretching mode at 1402 cm^{-1} is 4 cm^{-1} higher than the same mode in PhO•; and the CH bend at 1160 cm^{-1} is similarly close to its corresponding mode in PhO•. The two lowest frequency vibrations detected for TyrO• are the CCC trigonal bend at 975 cm^{-1} (15 cm^{-1} lower in frequency than the phenoxyl radical CCC trigonal bend) and the mode at 810 cm^{-1} composed of ring breathing and CC stretching (observed at 840 cm^{-1} in PhO•). Thus, the experimentally determined spin density ratios and the few experimentally measured vibrational frequencies for PhO• and TyrO• imply a very close correspondence between the spectral properties of the two radicals. Work presented here is intended to aid spectroscopic studies of TyrO• in proteins by demonstrating the similarities and differences between the structures, spin density distributions, and harmonic vibrational frequencies for phenoxyl and tyrosine phenoxyl radicals.

Computational Methods

Calculations for PhO• were performed by using unrestricted Hartree−Fock (UHF) and a variety of density-functional (DF) methods to determine the radical's optimum geometry and vibrational frequencies;[45] however, the flexibility of the TyrO• radical's peptide chain required a much more extensive search for stable conformations of TyrO•. These explorations to determine the lowest-energy conformations of the peptide chain for TyrO• were initiated by using the semiempirical molecular orbital method AM1,[46] as implemented in the program MOPAC 6.0.[47] First, we note that the calculated gas-phase structure for TyrO• was the neutral form, rather than the zwitterionic form of Tyr common in the solid state and in aqueous solution at neutral pH. A strong bonding interaction between the carboxyl hydrogen and the amino nitrogen appeared to fix the rotational orientation about the C′−C^{α} and C^{α}−N bonds, no matter which starting geometry was tried. Although this conformation about the C′−C^{α} and C^{α}−N bonds conflicts with the experimental gas-phase conformation of glycine[48−52] and with the conformation of glycine calculated by using *ab initio* and hybrid Hartree−Fock/density-functional methods,[53] the phenoxyl side chain that represents the focus of our TyrO• study is sufficiently remote from these atoms that our conclusions are not seriously affected. Thus, calculations were undertaken to optimize only the conformations about the C^{α}−C^{β} and C^{β}−C^{γ} bonds of TyrO•. Geometry optimizations were performed first with the conformation about C^{β}−C^{γ} fixed to maximize the separation between C^{α} and the phenoxyl side chain and with the C^{α}−C^{β} torsional angle constrained in 30° intervals from 0° to 360°. This series of calculations resulted in three low-energy conformations with substituents on C^{α} and C^{β} adopting staggered conformations. For each of the three low-energy geometries discovered by rotation about the C^{α}−C^{β} bond, geometry optimizations were next performed by constraining the C^{β}−C^{γ} bond in 30° intervals over its entire range of rotation. The AM1 conformational searches were then followed by geometry optimizations using the restricted open-shell Hartree−Fock (ROHF) method[54−56] with 3-21G and 6-31G basis sets[56] and starting from the three minimum-energy, AM1-derived structures. Finally, the conformation corresponding to the global energy minimum was subjected to geometry optimization by using DF methods with a 6-31G(d) basis set.[56] Because the spin density ratios and vibrational frequencies for PhO• calculated by using the SVWN method are more accurate than those from the HF methods,[45] the SVWN results are emphasized here.

Ab initio Hartree−Fock and density-functional calculations were accomplished by using the computer programs GAUSSIAN92/DFT[57] to solve the Hartree−Fock[56,58] or Kohn−Sham[59,60] equations. The UHF and DF calculations were performed by using a 6-31G(d) basis set[56,61] because it was previously found for PhO• that larger basis sets such as 6-31++G(d,p) and 6-311G(d,p) gave essentially the same structures, spin density distributions, and vibrational frequencies as the more economical 6-31G(d) basis.[45] In addition to various basis sets, several different DF methods were previously employed to study PhO• and

(45) Qin, Y.; Wheeler, R. A. *J. Chem. Phys.* **1995**, *102*, 1689−1698.
(46) Dewar, M. J. S.; Zoebisch, E. G.; Healy, E. F.; Stewart, J. J. P. *J. Am. Chem. Soc.* **1985**, *107*, 3902−3909.
(47) Stewart, J. J. P. *QCPE Bull.* **1983**, 455.
(48) Iijima, K.; Tanaka, K.; Onuma, S. *J. Mol. Struct.* **1991**, *246*, 257−266.
(49) Suenram, R. D.; Lovas, F. J. *J. Am. Chem. Soc.* **1980**, *102*, 7180−7184.
(50) Schäfer, L.; Sellers, H. L.; Lovas, F. J.; Suenram, R. D. *J. Am. Chem. Soc.* **1980**, *102*, 6566−6569.
(51) Brown, R. D.; Godfrey, P. D.; Storey, J. W. V.; Bassez, M.-P. *J. Chem. Soc., Chem. Commun.* **1978**, 547−548.
(52) Suenram, R. D.; Lovas, F. J. *J. Mol. Spectrosc.* **1978**, *72*, 372−382.
(53) Barone, V.; Adamo, C.; Lelj, F. *J. Chem. Phys.* **1995**, *102*, 364−370.
(54) McWeeny, R.; Diercksen, G. *J. Chem. Phys.* **1968**, *49*, 4852−4863.
(55) Hsu, H.; Davidson, E. R.; Pitzer, R. M. *J. Chem. Phys.* **1976**, *65*, 609−613.
(56) Hehre, W. J.; Radom, L.; Schleyer, P. V. R.; Pople, J. A. *Ab initio Molecular Orbital Theory*; Wiley, New York: 1986.
(57) Frisch, M. J.; Trucks, G. M.; Head-Gordon, M.; Gill, P. M. W.; Wong, M. W.; Foresman, J. B.; Johnson, B. G.; Schlegel, H. B.; Robb, M. A.; Replogle, E. R.; Gompters, R.; Andres, J. L.; Raghavachari, K.; Binkley, J. S.; Gonzalez, C.; Martin, R. L.; Fox, D. J.; Defrees, D. J.; Baker, J.; Stewart, J. J. P.; Pople, J. A. *GAUSSIAN92/DFT*; Gaussian Inc., 1992.
(58) Levine, I. N. *Quantum Chemistry*, 4th ed.; Prentice-Hall: Englewood Cliffs: NJ, 1991.
(59) Kohn, W.; Sham, L. J. *Phys. Rev. A* **1965**, *140*, 1133−1138.
(60) Hohenberg, P.; Kohn, W. *Phys. Rev. B* **1964**, *136*, 864−871.
(61) Davidson, E. R.; Feller, D. *Chem. Rev.* **1986**, *86*, 681−696.

related radicals. The results are summarized elsewhere.[45,62] The pure DF method that gave vibrational frequencies and spin density distributions in best agreement with experiment for radicals related to PhO•—Slater's local spin density exchange functional[63] and the local correlation functional of Vosko, Wilk, and Nusair[64] (abbreviated SVWN)—was employed here with the 6-31G(d) basis set to determine the lowest energy geometry and the corresponding vibrational frequencies for TyrO•. Slater's local spin density approximation for the exchange energy $E_X^{Slater}[\varrho]$[63] has the form

$$E_X^{Slater}[\varrho] = -\frac{9}{4}\alpha\left(\frac{3}{4\pi}\right)^{1/3}(\varrho_\alpha^{4/3} + \varrho_\beta^{4/3})$$

where ϱ_α is the density of electrons with spin $+^1/_2$ (α spin), ϱ_β is the density of electrons with spin $-^1/_2$ (β spin), and the proportionality constant α is $^2/_3$. The form for the local spin density approximation to the correlation energy proposed by Vosko, Wilk, and Nusair, $E_C^{VWN}[\varrho]$, is

$$E_C^{VWN}[\varrho] = (\varrho_\alpha + \varrho_\beta)\epsilon_C(x,\zeta)$$

where $x = (3/4\pi\varrho)^{1/6}$, $\zeta = (\varrho_\alpha - \varrho_\beta)/\varrho$, and $\varrho = \varrho_\alpha + \varrho_\beta$. In the above equation, the correlation potential is

$$\epsilon_C(x,\zeta) = \epsilon_C^P(x) + \epsilon_C^A(x)g(x)\left\{1 + \left[\frac{4}{9(2^{1/3}-1)}\frac{\epsilon_C^F(x) - \epsilon_C^P(x)}{\epsilon_C^A(x)} - 1\right]\zeta^4\right\}$$

where $g(\zeta) = {}^9/_8[(1+\zeta)^{4/3} + (1-\zeta)^{4/3} - 2]$ and the various forms of ϵ_C are

$$\epsilon_C(x) = A\left\{\ln\frac{x^2}{X(x)} + \frac{2b}{Q}\tan^{-1}\frac{Q}{2x+b} - \frac{bx_0}{X(x_0)}\left[\ln\frac{(x-x_0)^2}{X(x)} + \frac{2(2x_0+b)}{Q}\tan^{-1}\frac{Q}{2x+b}\right]\right\}$$

with $X(x) = x^2 + bx + c$, $Q = (4c - b^2)^{1/2}$ and with A, b, c, and x_0 assuming different values for each individual ϵ_C.

The spin-unrestricted formalism was used in solving the Hartree—Fock and Kohn—Sham equations. Integrals required to solve the Kohn—Sham DF equations were evaluated by numerical quadrature on a grid of points by using standard methods described elsewhere.[65,66] Berny's optimization algorithm[67] in internal coordinates was used to fully optimize all phenoxyl radical geometries in C_{2v} symmetry, whereas TyrO• geometries were optimized in internal coordinates with no symmetry constraints. Analytical first and numerical second derivatives of the energy were computed for calculating harmonic force constants. Harmonic vibrational frequencies were calculated for the lowest energy geometry, at each level of theory, for PhO• and for TyrO•. Mode assignments were performed graphically and with the aid of a variety of isotopic substitutions and total energy distributions[68,69] obtained by reformatting the Hessian matrix produced by GAUSSIAN92/DFT, reading the Hessian matrix into the program GAMESS,[70,71] and using the GAMESS program to calculate total energy distributions. Internal coordinates for total energy distributions were chosen according to the method suggested by Boatz and Gordon.[72]

Spin densities reported in this paper were obtained by using Mulliken population analysis.[73] Although atomic charges derived from Mulliken population analysis are generally believed to vary for different basis sets and different computational levels,[58,74] for the phenoxyl radical we find that computed spin densities are qualitatively correct and change by less than 0.06 for any atom when we employ other methods and larger basis sets.[62] Methods tested include Becke's gradient-corrected exchange functional[75] with Lee, Yang, and Parr's gradient-corrected correlation functional[76] and the three-parameter, hybrid Hartree—Fock/density-functional "B3LYP" method.[77] Basis sets employed include diffuse functions (the 6-31++G(d,p) basis) and split-valence basis plus polarization functions (6-311G(d,p) and 6-311G(2d,2p) basis sets). The good agreement between experimental and calculated spin densities achieved with the SVWN method, as well as the insensitivity of computed spin densities to method and basis set, contrasts with the marked dependence of hyperfine properties for the non-hydrogen atoms of phenoxyl[62] and other radicals[78—80] on the computational method as well as the basis set used.

Phenoxyl and Tyrosine Phenoxyl Radical Structures and Spin Densities

The three lowest energy conformations of the TyrO• radical are illustrated by the Newman projections viewed along the C^α—C^β bond, shown in **4a**, **4b**, and **4c**. **4** also lists the energy of each conformation (in atomic units), calculated at the SVWN/6-31G(d) level. Conformation **4a** has the lowest energy, but

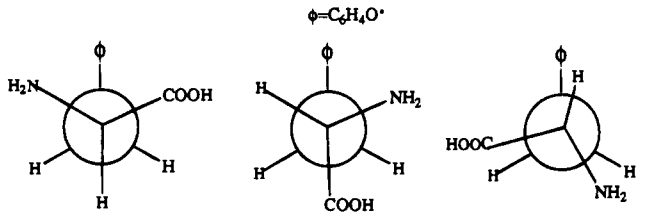

E_{SVWN}(Hartree)= -626.0153554	-626.0122800	-626.0104375
ΔE_{SVWN}(kcal/mol)= 0.0	1.93	3.09
a	**b**	**c**

4

4b is less than 2 kcal/mol higher in energy and **4c** is within 3 kcal/mol of the lowest energy conformation. Although it appears unusual that the lowest energy conformation would place the phenoxyl ring gauche to both the CO_2H and NH_2 groups, the conformation in **4a** is observed in the neutron diffraction structure of zwitterionic L-tyrosine[81] and conformation **4a** is consistently attained with different methods and different basis sets including ROHF/3-21G, ROHF/6-31G, and SVWN/6-31G(d). Moreover, qualitative conclusions concerning the similarities and differences between PhO• and the phenoxyl side chain of TyrO• are the same for all three conformations, so we emphasize our results for the lowest energy conformation, **4a**, in the following discussion.

(62) Qin, Y.; Wheeler, R. A. Work in progress.
(63) Slater, J. C. *Quantum Theory of Molecules and Solids*; McGraw-Hill: New York, 1974; Vol. 4.
(64) Vosko, S. H.; Wilk, L.; Nusair, M. *Can. J. Phys.* **1980**, *58*, 1200—1211.
(65) Becke, A. D. *J. Chem. Phys.* **1988**, *88*, 2547—2553.
(66) Johnson, B. G.; Gill, P. M. W.; Pople, J. A. *J. Chem. Phys.* **1993**, *98*, 5612—5626.
(67) Schlegel, H. B. *J. Comp. Chem.* **1982**, *3*, 214—218.
(68) Pulay, P.; Torok, F. *Acta Chim. Acad. Sci. Hung.* **1965**, *47*, 273—279.
(69) Keresztury, G.; Jalsovszky, G. *J. Mol. Struct.* **1971**, *10*, 304—305.
(70) Schmidt, M. W.; Baldridge, K. K.; Boatz, J. A.; Jensen, J. H.; Koseki, S.; Gordon, M. S.; Nguyen, K. A.; Windus, T. L.; Elbert, S. T. *QCPE Bull.* **1990**, *10*, 52.
(71) Dupuis, M.; Spangler, D.; Wendoloski, J. J. *National Resource for Computations in Chemistry Software Catalog, Program QG01*; University of California; Berkeley, CA, 1980.
(72) Boatz, J. A.; Gordon, M. S. *J. Phys. Chem.* **1989**, *93*, 1819—1826.
(73) Mulliken, R. S. *J. Chem. Phys.* **1955**, *23*, 1833—1840.
(74) Mulliken, R. S.; Ermler, W. C. *Diatomic Molecules*; Academic: New York, 1977.
(75) Becke, A. D. *Phys. Rev. A* **1988**, *38*, 3098—3100.
(76) Lee, C.; Yang, W.; Parr, R. G. *Phys. Rev. B* **1988**, *37*, 785—789.
(77) Stephens, P. J.; Devlin, F. J.; Chabalowski, C. F.; Frisch, M. J. *J. Phys. Chem.* **1994**, *98*, 11623—11627.
(78) Adamo, C.; Barone, V.; Fortunelli, A. *J. Phys. Chem.* **1994**, *98*, 8648—8652.
(79) Eriksson, L. A.; Malkina, O. L.; Malkin, V. G.; Salahub, D. R. *J. Chem. Phys.* **1994**, *100*, 5066—5075.
(80) Eriksson, L. A.; Malkin, V. G.; Malkina, O. L.; Salahub, D. R. *J. Chem. Phys.* **1993**, *99*, 9756—9763.
(81) Frey, M. N.; Koetzle, T. F.; Lehmann, M. S.; Hamilton, W. C. *J. Chem. Phys.* **1973**, *58*, 2547—2556.

Table 3. Bond Distances for Phenoxyl and Tyrosine Phenoxyl Radicals Calculated by Using the SVWN Density−Functional Method with the 6-31G(d) Basis Set

bond	TyrO•	PhO•
$C'-O^1$	1.214	
$C'-O^2$	1.320	
O^2-H^{O2}	1.026	
$C'-C^\alpha$	1.535	
$C^\alpha-N$	1.452	
$N-H^{N1}$	1.031	
$N-H^{N2}$	1.024	
$C^\alpha-H$	1.107	
$C^\beta-H^{\beta1}$	1.105	
$C^\beta-H^{\beta2}$	1.105	
$C^\alpha-C^\beta$	1.530	
$C^\beta-C^\gamma$	1.484	
$C^\gamma-C^{\delta1}$	1.410	1.403
$C^{\delta1}-C^{\epsilon1}$	1.373	1.373
$C^{\epsilon1}-C^\zeta$	1.445	1.445
$C^\zeta-C^{\epsilon2}$	1.445	1.445
$C^{\epsilon2}-C^{\delta2}$	1.371	1.373
$C^{\delta2}-C^\gamma$	1.412	1.403
$C^{\delta1}-H^{\delta1}$	1.099	1.096
$C^{\epsilon1}-H^{\epsilon1}$	1.096	1.095
$C^\zeta-O^\eta$	1.252	1.253
$C^{\epsilon2}-H^{\epsilon2}$	1.095	1.095
$C^{\delta2}-H^{\delta2}$	1.098	1.096

Table 3 presents a comparison of bond distances for PhO• and the lowest energy conformation of the TyrO• radical, calculated by using the SVWN density-functional method. The structures were also optimized by using the *ab initio* UHF method, but we have previously tested the reliability of the SVWN and UHF methods for PhO• and reported[45] that the SVWN method yields more accurate spin densities and better bond distances between non-hydrogen atoms, within an average of 0.009 Å of a published structure calculated by using the more sophisticated CASSCF method[82−89] with a larger 6-311G(2d,p) basis set.[90] The SVWN method indicates that PhO• has a $C^\zeta O$ bond distance of 1.253 Å, closer to the C=O double bond distance of 1.225 Å observed for *p*-benzoquinone[91] than to the 1.381 Å C−O single bond distance of phenol.[92,93] The $C^\zeta O$ bond of PhO• thus appears to have substantial double bond character. Similarly, the calculated $C^\zeta C^{\epsilon1}$ and $C^\zeta C^{\epsilon2}$ distance of 1.445 Å is shorter than the corresponding distance in *p*-benzoquinone (1.481 Å), but not as short as the carbon−carbon distance in benzene (1.396 Å)[94] or phenol (1.399 Å). The $C^{\epsilon1}C^{\delta1}$ and $C^{\epsilon2}C^{\delta2}$ distances in PhO• are shorter still, 1.373 Å, and are almost midway between the carbon−carbon distances in benzene or phenol (1.399 Å) and the C=C double bond distances observed for *p*-benzoquinone (1.344 Å). The carbon−carbon bonds most remote from the oxygen in PhO•, $C^{\delta1}C^\gamma$, and $C^{\delta2}C^\gamma$ display bond distances of 1.403 Å, close to the corresponding carbon−carbon distances in phenol (1.399 Å) or in benzene. Thus PhO• displays structural features intermediate between those of a benzenoid or phenolic structure (see **2a**) and those expected for a quinoidal molecule (**2b**) such as *p*-benzoquinone. Specifically, the $C^\zeta O^\eta$ distance and two carbon−carbon distances show substantial double bond character, similar to quinones, but the carbon−carbon bonds nearest to and farthest from the oxygen display distances expected for a benzenoid or phenolic ring.

The bond distances calculated for TyrO• and displayed in Table 3 demonstrate the pronounced similarity between the structures of phenoxyl and tyrosine side chain phenoxyl radicals. First, the $C^\zeta O^\eta$ distance calculated for TyrO•, 1.252 Å, is only 0.001 Å shorter than that calculated for the phenoxyl radical. Next, the $C^\zeta C^{\epsilon1}$ and $C^\zeta C^{\epsilon2}$ distances are equal to each other and are exactly the same as the corresponding distance for PhO•. The $C^{\epsilon1}C^{\delta1}$ and $C^{\epsilon2}C^{\delta2}$ distances of TyrO• are slightly different from each other due to the asymmetry of the peptide chain, but their average, 1.372 Å, is again only 0.001 Å shorter than the corresponding calculated distance for PhO•. Although the $C^{\delta1}C^\gamma$ and $C^{\delta2}C^\gamma$ bonds are closest to the peptide chain and might therefore be expected to show distances that differ the most from those of PhO•, the similarity between TyrO• and PhO• is once again striking. The $C^{\delta1}C^\gamma$ (1.410 Å) and $C^{\delta2}C^\gamma$ (1.412 Å) distances in TyrO• are only 0.007 and 0.009 Å longer, respectively, than distances between the same carbons in PhO•. Consequently, the peptide chain appears to perturb the structure of the phenoxyl radical side chain of TyrO• very little.

The calculated structural similarities between PhO• and TyrO• evident in Table 3 are also reflected in the calculated spin density distributions shown in **5**. Although to our knowledge no experimental spin densities are currently available for PhO•, experimentally-derived *ratios* of spin densities on the carbon atoms of PhO• given in footnote *a* for Table 1[43,44] are accurately reproduced by the SVWN computational method (calculated spin ratios are $\varrho(C^\gamma)/\varrho(C^\epsilon) = 1.3$ and $\varrho(C^\gamma)/\varrho(C^\delta) = 5.3$). For comparison with the computed spin densities for PhO• displayed in **5a**, the sketch **5b** shows calculated spin densities for TyrO•

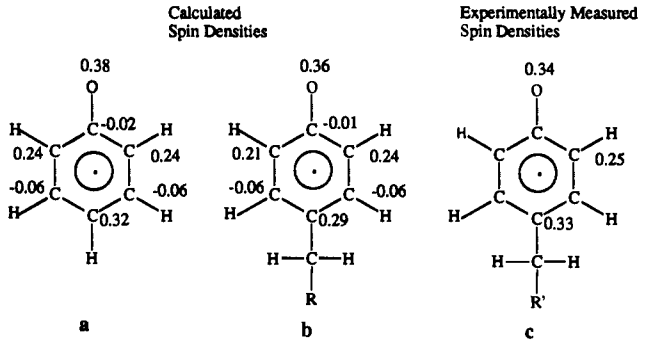

5

and **5c** shows experimentally-derived spin densities for TyrO• in mouse ribonucleotide reductase.[35] Calculated spin densities for TyrO• are evidently very close to those for PhO•. The largest calculated spin densities for PhO• (0.38) and TyrO• (0.36) appear on the phenoxyl oxygen atom and are almost identical. Likewise, the smallest spin densities occur on C^ζ for both radicals (−0.01 for PhO• and for TyrO•). The carbon atoms *ortho* to C^ζ ($C^{\epsilon1}$ and $C^{\epsilon2}$) carry a large amount of unpaired, electronic spin for both PhO• (0.24) and TyrO• (0.21 and 0.24) radicals, whereas spin densities at the *meta*-carbons $C^{\delta1}$ and $C^{\delta2}$ are once again low (−0.06 for both PhO• and TyrO•).

(82) Roos, B. O.; Taylor, P. R.; Siegbahn, P. E. M. *Chem. Phys.* **1980**, *48*, 157−173.
(83) Roos, B. O. *Adv. Chem. Phys.* **1987**, *69*, 399−445.
(84) Siegbahn, P. E. M.; Heiberg, A.; Roos, B. O. *Phys. Scr.* **1980**, *21*, 323−327.
(85) Siegbahn, P. E. M.; Almlöf, J.; Heiberg, A.; Roos, B. O. *J. Chem. Phys.* **1981**, *74*, 2384−2396.
(86) Ruedenberg, K.; Sundberg, K. R. In *Quantum Science*; Calais, J.-L., Goscinski, O., Linderberg, J., Öhrn, Y., Eds.; Plenum: New York, 1976; pp 505−515.
(87) Ruedenberg, K.; Cheung, L. M.; Elbert, S. T. *Int. J. Quantum Chem.* **1979**, *16*, 1069−1101.
(88) Ruedenberg, K.; Schmidt, M. W.; Gilbert, M. M.; Elbert, S. T. *Chem. Phys.* **1982**, *71*, 41−49, 65−78.
(89) Cheung, L. M.; Sundberg, K. R.; Ruedenberg, K. *Int. J. Quantum Chem.* **1979**, *16*, 1103−1139.
(90) Chipman, D. M.; Liu, R.; Zhou, X.; Pulay, P. *J. Chem. Phys.* **1994**, *100*, 5023−5035.
(91) Hagen, K.; Hedberg, K. *J. Chem. Phys.* **1973**, *59*, 158−162.
(92) Portalone, G.; Schultz, G.; Domenicano, A.; Hargittai, I. *Chem. Phys. Lett.* **1992**, *197*, 482−488.
(93) Larsen, N. W. *J. Mol. Struct.* **1979**, *51*, 175−190.
(94) Cabana, A.; Bachand, J.; Giguere, J. *Can. J. Phys.* **1974**, *52*, 1949−1955.

Finally, large spin densities appear again at the carbon *para*- to the oxygen atom (C^{γ}) for both PhO• (0.32) and TyrO• (0.29) radicals. Thus, the calculated spin densities on the phenoxyl side-chain of TyrO• are almost identical to those calculated for PhO•. Moreover, calculated TyrO• spin densities agree very well with experimental spin densities displayed in **5c**.[35] Compared with other experimentally-derived spin densities for TyrO•[6,33,34] shown in Table 1, however, the SVWN method appears to place too large a spin density on the phenoxyl oxygen, at the expense of unpaired spin at C^{γ}. Nonetheless, the calculated pattern of high and low spin density alternation evident in **5** for the carbon rings of PhO• and TyrO• is characteristic of odd-alternant cyclic polyenes,[39] agrees with experimental observations for both radicals,[6,33-35,43,44] and is consistent with the relative magnitudes of atomic orbital coefficients for PhO• displayed in **6**. It is interesting to note

6

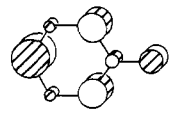

that calculated spin densities on the phenoxyl side chain of TyrO• account for one entire unpaired electron and we find no evidence in our calculations for spin delocalization onto the peptide chain. In conclusion, the calculated structures and spin density distributions for TyrO• and PhO• are very similar.

Harmonic Vibrations of Phenoxyl and Tyrosine Phenoxyl Radicals

Several calculated vibrational frequencies for TyrO•, like its side chain structure and spin density distribution, show a remarkable similarity to corresponding features of PhO•. Figure 1 illustrates the calculated vibrational modes of TyrO• whose frequencies have been experimentally determined, but the corresponding modes of PhO• are not displayed because they have been described elsewhere[45] and they are extremely similar to the sketches shown for TyrO•. Figure 1 also includes Wilson notation[95,96] for the calculated modes of PhO•, as well as experimental[30,36-38] and calculated vibrational frequencies for both PhO• and TyrO• to emphasize their similarities further. We note that it is customary to scale vibrational frequencies calculated by using *ab initio* quantum chemical methods to bring them into better agreement with experiment[97-100] and that scaling factors for frequencies or force constants derived from some density-functional methods have recently been published,[101] but we prefer to report unscaled frequencies.

Comparing experimental and *unscaled*, calculated harmonic vibrational frequencies for PhO• and TyrO• reveals an average error in our calculations of 31 cm^{-1} for PhO• and 26 cm^{-1} for TyrO•. For PhO•, the highest-frequency, experimentally-observed vibrational mode, corresponding to the TyrO• mode sketched in the upper left corner of Figure 1, is described as a

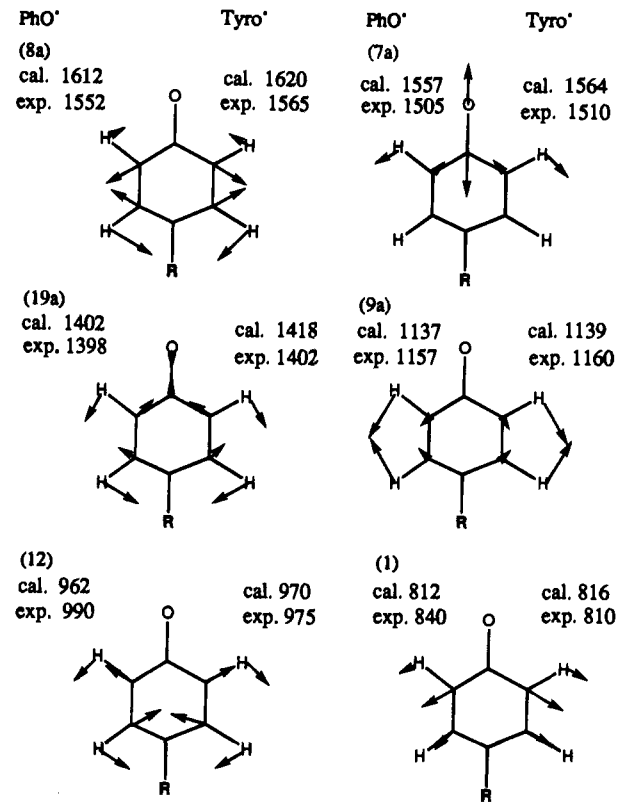

Figure 1. Vibrational modes of tyrosine phenoxyl radicals for modes whose frequencies were experimentally measured. Calculated and experimental frequencies for phenoxyl and tyrosine phenoxyl radicals are shown. Wilson mode descriptions[95,96] for phenoxyl radical modes are given in parentheses.

CC stretching mode (Wilson mode 8a) at 1552 cm^{-1} and is calculated to appear at a frequency of 1612 cm^{-1}. Immediately below is the CO stretching mode (7a) observed at 1505 cm^{-1} and calculated at 1557 cm^{-1}. A mixed CH bend/CC stretch (19a) shows up at 1398 cm^{-1}, and its frequency is well-reproduced by our calculations at 1402 cm^{-1}. Next lowest in frequency, but not shown in the Figure, is a B_2 symmetry mode composed of CC stretching and CH bending motions (Wilson mode 14), measured at 1331 cm^{-1} and calculated at 1371 cm^{-1}. A CH bend of A_1 symmetry (9a) appears next, at 1157 cm^{-1} (with a calculated frequency of 1137 cm^{-1}), then a CH bending plus ring breathing mode occurs at 1050 cm^{-1} (calculated at 1015 cm^{-1} and assigned by us to Wilson mode 18a). The three lowest-frequency, experimentally-observed modes for PhO• involve in-plane motions of the carbon ring: a CCC trigonal bending mode appears at 990 cm^{-1} (962 cm^{-1} calculated frequency, mode 12), a ring breathing/CCC bending mode shows up at 840 cm^{-1} (calculated at 812 cm^{-1}, Wilson mode 1), and the lowest-frequency mode, observed at 528 cm^{-1} (calculated at 518 cm^{-1}), also involves CCC bending (6a). We note that the three modes of A_1 symmetry calculated to appear at 1015, 962, and 812 cm^{-1} are relatively close in frequency and are somewhat mixed, so our assignments appear to differ from those of Tripathi and Schuler.[36-38] The different assignments were described in previous work[45] and may reflect limitations of our calculations, although the calculated mode assignments are consistent for every computational method we employed.[45] Moreover, our placement of the Wilson mode 1 slightly above 800 cm^{-1} is consistent with observations of Johnson et al. for PhO•.[30] In summary, the unscaled harmonic vibrational frequencies calculated for PhO• by using the SVWN method differ from experiment by −3.3% to +3.9% and are therefore more

(95) Varsanyi, G. *Vibrational Spectra of Benzene Derivatives*; Academic: New York, 1969; Chapter 3.
(96) Dollish, F. R.; Fateley, W. G.; Bentley, F. F. *Characteristic Raman Frequencies of Organic Compounds*; Wiley-Interscience: New York, 1974; Chapter 13.
(97) Blom, C. E.; Altona, C. *Mol. Phys.* **1976**, *31*, 1377−1391.
(98) Pople, J. A.; Schlegel, H. B.; Krishnan, R.; Defrees, D. J.; Binkley, J. S.; Frisch, M. J.; Whiteside, R. A.; Hout, R. F.; Hehre, W. J. *Int. J. Quantum Chem. Symp.* **1981**, *15*, 269−278.
(99) Pulay, P.; Fogarasi, G.; Pongor, G.; Boggs, J. E.; Vargha, A. *J. Am. Chem. Soc.* **1983**, *105*, 7037−7047.
(100) Pople, J. A.; Scott, A. P.; Wong, M. W.; Radom, L. *Isr. J. Chem.* **1993**, *33*, 345−350.
(101) Rauhut, G.; Pulay, P. *J. Phys. Chem.* **1995**, *99*, 3093−3100.
(102) Boesch, S. E.; Wheeler, R. A. *J. Phys. Chem.* **1995**, in press.
(103) Hienerwadel, R.; Boussac, A.; Breton, J.; Mäntele, W.; Berthomieu, C. *Biophys. J.* **1995**, *68*, A93.

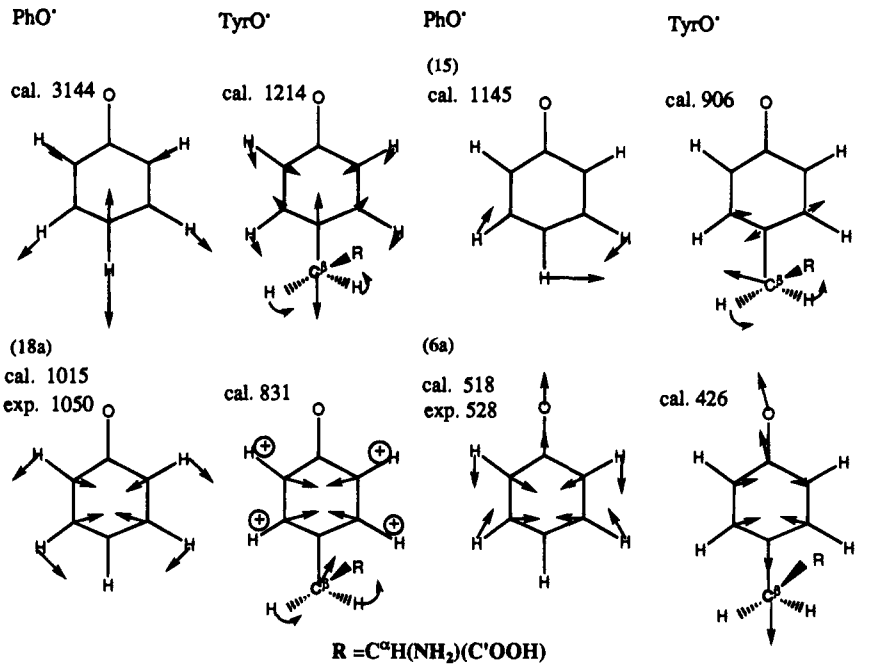

Figure 2. Vibrational modes and frequencies for phenoxyl and tyrosine phenoxyl radicals that differ the most. Wilson mode descriptions[95,96] for phenoxyl radical modes are given in parentheses.

accurate than those obtained by other calculations that require equivalent computational effort, such as the UHF method.[45]

Six of the same modes observed experimentally for PhO• have been detected experimentally for the TyrO• radical,[30] and their corresponding frequencies are also listed in Figure 1. Thus, the ring carbon−carbon stretching mode measured at 1565 cm^{-1} for TyrO• (8a) appears at 1620 cm^{-1} in our calculations, the ring $C^{\zeta}O^{\eta}$ stretch observed at 1510 cm^{-1} (7a) has a calculated frequency of 1564 cm^{-1}, and the ring CH bending/CC stretching mode at 1402 cm^{-1} for TyrO• is calculated to appear at 1418 cm^{-1}. Our assignment of this frequency to Wilson mode 19a contrasts with that of Johnson et al.,[30] but it is consistent with the assignment of Tripathi and Schuler for PhO•.[38] A ring CH bend was also measured at 1160 cm^{-1} (9a) and calculated at 1139 cm^{-1}. The CCC trigonal bend of TyrO• was observed at 975 cm^{-1} and calculated at 970 cm^{-1} (mode 12) and a mode attributed to ring breathing/$C'C^{\alpha}$ stretching was measured at a frequency of 810 cm^{-1} (mode 1) and calculated at 816 cm^{-1}. As for PhO•, the band corresponding to our calculated Wilson mode 12 for TyrO• is closest to the measured frequency assigned to mode 18a. Thus, the SVWN density-functional method yields the same mode assignments for TyrO• as for PhO• and gives unscaled harmonic vibrational frequencies for TyrO• with an accuracy similar to that for the vibrational frequencies of PhO• (within −1.8% to +3.5% of experiment).

Even though the unscaled, calculated frequencies for PhO• and TyrO• shown in Figure 1 differ from experiment by as much as 60 cm^{-1}, the SVWN density-functional method yields unscaled, harmonic vibrational frequencies in better agreement with experiment than comparable quantum chemical methods accessible for such large molecules. The SVWN method also gives frequency shifts from PhO• to TyrO• in the same directions as experiment and by similar amounts for modes localized on the phenoxyl ring. For example, the CC stretch observed at 1552 cm^{-1} for PhO• shifts up in frequency by 13 cm^{-1}, to 1565 cm^{-1} in TyrO•, whereas the calculated frequency increase, 8 cm^{-1}, is similar. Likewise, the $C^{\zeta}O^{\eta}$ stretch is observed to increase in frequency by 5 cm^{-1} and is calculated to go up by 7 cm^{-1} from PhO• to TyrO•, the ring bend/CC stretch measured at 1398 cm^{-1} increases by 4 cm^{-1} according to experiment and by 16 cm^{-1} in the calculations, and the ring CH bend was observed to go up by 3 cm^{-1} and calculated to increase 2 cm^{-1}. In contrast, the CCC trigonal bending and ring breathing/CCC bending modes are observed to decrease in frequency by 15 and 30 cm^{-1}, respectively, while our calculations yield a frequency *increase* of 8 cm^{-1} for the CCC trigonal bend and 4 cm^{-1} for the ring breathing/CCC bending mode. We believe this discrepancy could be due to different conformations for TyrO• in the calculations and the experiments—calculations were performed for isolated TyrO•, whereas experiments detected "tyrosine transients" in solution.[30] We expect these modes, which are experimentally known to be sensitive to amino acid conformation for tyrosine[30] and show some mixing between ring modes and modes of the peptide chain in the calculation, to show the largest discrepancies between calculation and experiment. Calculations thus reproduce the approximate frequency change upon comparing PhO• and TyrO• frequencies for the important CC stretching, CO stretching, and CH bending/CC stretching modes; however, experiment and calculation differ on the shift for the CCC trigonal bend and the ring breathing/CCC bending modes. Nonetheless, SVWN density-functional calculations appear capable of giving the approximate frequency range to search for currently unobserved vibrational modes such as those discussed next.

Figure 1 shows sketches and frequencies for selected vibrational modes of TyrO• and PhO• to emphasize their similarities; Figure 2 displays sketches of the TyrO• modes whose frequencies differ the most from those of the corresponding PhO• modes (also shown in Figure 2). The upper left corner of Figure 2 contrasts one A_1 symmetry CH stretching mode of PhO• with the corresponding mode of TyrO•. For PhO•, the mode at 3144 cm^{-1} involves a substantial contribution from the hydrogen atom replaced by the peptide chain of TyrO•. For TyrO• the mode's frequency has therefore shifted to 1214 cm^{-1} and now includes the $C^{\beta}H_2$ wagging motion in addition to $C^{\beta}C^{\gamma}$ stretching and CH bending. The A_1 symmetry ring breathing/CH bending mode with a calculated frequency of 1015 cm^{-1} for PhO• also shifts substantially, to 831 cm^{-1}, as it takes on some ring CH wagging and $C^{\beta}H_2$ rocking motion in TyrO•. Phenoxyl radical modes calculated to appear at 518 cm^{-1} (6a) and 1145 cm^{-1} (mode 15) also display very different frequencies in TyrO•. The $C^{\delta 1}C^{\gamma}C^{\delta 2}$ in-plane bending mode at 518 cm^{-1} in PhO• appears

Table 4. Symmetries, Approximate Mode Descriptions, and Vibrational Frequencies for PhO• and TyrO• [a]

tyrosine radical					phenoxyl radical	
approx description	exp[b]	calcd	sym	approx description	exp[c]	calcd
ring CH str		3153	A_1	CH str		3155
ring $C^{\beta}C^{\gamma}$ str/$C^{\beta}H_2$ wag/ring CH bend		1214	A_1	CH str		3144
ring CH str		3093	A_1	CH str		3123
ring CC str	**1565**	**1620**	A_1	CC str	**1552**	**1612**
ring $C^{\zeta}O^{\eta}$ str	**1510**	**1564**	A_1	$C^{\zeta}O^{\eta}$ str	**1505**	**1557**
ring CH bend/CC str	**1402**	**1418**	A_1	**CH bend/CC str**	**1398**	**1402**
ring CH bend	**1160**	**1139**	A_1	**CH bend**	**1157**	**1137**
ring breath/ring CH wag/$C^{\alpha}NC^{\beta}$ bend		831	A_1	**ring breath/CH bend**	**1050**	**1015**
CCC **trig bend**	**975**	**970**	A_1	CCC **trig bend**	**990**	**962**
ring breath/$C^{\alpha}C$ str	**810**	**816**	A_1	**ring breath/CCC bend**	**840**	**812**
$C^{\delta 1}C^{\gamma}C^{\delta 2}$ bend/NH_2 wag/ring breathing		426	A_1	$C^{\delta 1}C^{\gamma}C^{\delta 2}$ **bend**	**528**	**518**
ring HCCH torsion		935	A_2	HCCH torsion		933
ring CH wag		775	A_2	CH wag		767
ring def/$C^{\beta}H_2$ rock		362	A_2	ring def		356
ring HCCH torsion		964	B_1	HCCH torsion		960
ring CH wag/$C^{\gamma}C^{\beta}$ wag		857	B_1	CH wag		895
ring CH wag/O1C'O2 bend/ring torsion		781	B_1	CH wag/ring torsion		780
C^{β}-ring wag/CH wag		600	B_1	CH wag		632
($C^{\epsilon 1}C^{\gamma}C^{\epsilon 2}$/$C^{\delta 1}C^{\zeta}C^{\delta 2}$) out-of-plane bend/ring (CH+$C^{\zeta}O^{\eta}$) wag			B_1	($C^{\epsilon 1}C^{\gamma}C^{\epsilon 2}$+$C^{\delta 1}C^{\zeta}C^{\delta 2}$) out-of-plane bend/$C^{\zeta}O^{\eta}$ wag		
ring boat def/$C^{\zeta}O^{\eta}$ wag/$C^{\alpha}C^{\beta}C^{\gamma}$ bend/NH_2 rock		158	B_1	ring boat def/$C^{\zeta}O^{\eta}$ wag		184
CH str		3152	B_2	CH str		3153
CH str		3121	B_2	CH str		3128
ring CC str/CH bend		1509	B_2	CC str/CH bend		1544
ring CC str		1466	B_2	CH bend/CC str		1465
ring CC str/$C^{\beta}H_2$ twist/$C^{\alpha}H$ wag		1350	B_2	CC str/**CH bend**	**1331**	**1371**
ring CH bend/ring CC str/$C^{\beta}H_2$ twist		1247	B_2	CC str/CH bend		1253
($C^{\beta}H_2$)C^{γ} rock/NH_2 wag		906	B_2	$C^{\gamma}H^{\gamma}$ bend/CC str		1145
ring CH bend		1076	B_2	CH bend/CC str		1068
ring CCC in-plane bend		608	B_2	CCC in-plane bend		582
$C^{\zeta}O^{\eta}$ bend/$C^{\beta}H_2$ rock		434	B_2	$C^{\zeta}O^{\eta}$ bend		430

[a] Modes where frequencies were experimentally measured are shown in bold type. [b] Reference 30. [c] References 37 and 38.

at 426 cm^{-1} and includes NH_2 wagging and ring breathing motions in TyrO•, whereas the CH bending component of the PhO• mode at 1145 cm^{-1} is mixed with $C^{\beta}H_2$ rocking and NH_2 wagging motions in TyrO•. Thus, the four modes whose frequencies differ the most between PhO• and TyrO• involve large motions of the PhO• hydrogen that is replaced by the peptide chain of TyrO• or, in two cases, involve substantial hindrance of CH bending due to the peptide chain.

We should also note that several of our mode assignments for PhO• differ from those obtained by using more sophisticated computational methods[90] and the discrepancies are discussed in a previous publication.[45] Briefly, the modes we calculate to appear at 1015 and 962 cm^{-1} are assigned to CH bending/ring breathing (mode 18a) and CCC trigonal bending motions (mode 12), respectively. Previous workers reversed this assignment,[90] but only after the in-plane force constants were rescaled to fit experimental frequencies.[36-38] Thus, the relative frequencies of these two modes depend upon the adequacy of the scaling factors employed. In addition, we assign the mode calculated at 1371 cm^{-1} to a CC stretching/CH bending mode (mode 14), whereas the *ab initio* calculations placed mode 14 at a scaled frequency of 1260 cm^{-1} and found no satisfactory explanation for the weak band observed at 1331 cm^{-1}. Although specific assignments for these modes are important for very exact spectroscopic work, they are not critical for the comparisons of PhO• and TyrO• emphasized in this contribution.

Table 4 shows a comparison of all calculated, harmonic vibrational frequencies for TyrO• and PhO•. Modes whose frequencies have been experimentally determined are given in bold type in the table. Among the modes of A_1 symmetry for PhO•, only the frequencies for the CH stretching modes were not measured experimentally and they all appear near 3100–3200 cm^{-1}. Our experience with other molecules such as phenol[62] and *p*-benzoquinone[102] leads us to believe that these calculated CH stretching frequencies may be as much as 100–200 cm^{-1} too high. For TyrO•, the modes corresponding to phenoxyl radical's A_1 symmetry CH stretching modes also appear near the same frequency range, with one exception. This exception and other TyrO• modes corresponding to the A_1 symmetry modes of PhO• have already been discussed and will not be described again. For the A_2 and B_1 symmetry modes of PhO•, the corresponding modes of TyrO• also appear at similar frequencies. The largest calculated frequency shift for the A_2 or B_1 modes, −38 cm^{-1}, occurs for a B_1 symmetry CH wag of PhO•. In TyrO•, this mode is mixed with $C^{\gamma}C^{\beta}$ wagging motion and shifts from 895 cm^{-1} in PhO• to 857 cm^{-1} in TyrO•. Other B_1 symmetry modes that show relatively large frequency shifts include another CH wag (632 cm^{-1} in PhO• and 600 cm^{-1} in TyrO•), the ring boat bend/$C^{\zeta}O^{\eta}$ wag (184 cm^{-1} in PhO• and 158 cm^{-1} in TyrO•), and the CCC out-of-plane bend/$C^{\zeta}O^{\eta}$ wag (465 cm^{-1} in PhO• and 481 cm^{-1} in TyrO•). Most calculated frequencies for the B_2 symmetry modes of PhO• also show small frequency shifts. In particular, Wilson mode 3 is very similar to mode 14 and is calculated to appear at 1253 cm^{-1} for PhO• and 1247 cm^{-1} for TyrO•. Among the other modes not discussed previously, the largest frequency differences between the phenoxyl radical's B_2 modes and the corresponding mode of TyrO• are the CC stretch/CH bend at 1544 cm^{-1} in PhO• and 1509 cm^{-1} in TyrO•, the CC stretch/CH bend at 1371 cm^{-1} in PhO• and 1350 cm^{-1} in TyrO•, and the CCC in-plane bend at 582 cm^{-1} for PhO• and calculated at 608 cm^{-1} for TyrO•. Thus, modes of PhO• that show the greatest frequency shifts upon replacing the phenoxyl hydrogen by the TyrO• peptide chain involve the phenoxyl hydrogen atom directly, bending motions of hydrogens adjacent to the TyrO• peptide chain, or out-of-plane ring torsions. Modes involving the phenoxyl hydrogen atom are naturally expected to display large frequency shifts due to different force constants resulting from differences in CH versus CC bonding, as well as the larger mass of the peptide chain compared to hydrogen. On the other hand, CH and out-of-plane ring bending modes differ between PhO• and TyrO• because of interactions between atoms of the ring and

Table 5. Approximate Mode Descriptions, Calculated Vibrational Frequencies for TyrO•, and Isotopic Frequency Shifts for TyrO•-d_7 and TyrO•-$^{13}C_6$

approx description	h	d_7	$\nu_h - \nu_{d7}$	$^{13}C_6$	$\nu_h - \nu_{^{13}C_6}$
ring CH str	3153	2336	817	3143	10
ring $C^{\beta}C^{\gamma}$ str/$C^{\beta}H_2$ wag/ring CH bend	1214	1171	46	1195	19
ring CH str	3093	2284	809	3083	10
ring CC str	1620	1591	29	1564	56
ring $C^{\zeta}O^{\eta}$ str	1564	1553	11	1523	41
ring CH bend/CC str	1418	1186	232	1389	29
ring CH bend	1139	815	324	1135	4
ring breath/ring CH wag/$c^{\alpha}NC^{\beta}$ bend	831	797	34	822	9
CCC trig bend	970	862	108	944	26
ring breath/$C^{\alpha}C$ str	816	767	49	796	20
$C^{\delta 1}C^{\gamma}C^{\delta 2}$ bend/NH_2 wag/ring breathing	426	411	15	422	4
ring HCCH torsion	935	751	184	927	8
ring CH wag	775	602	173	769	6
ring def/$C^{\beta}H_2$ rock	362	320	42	347	15
ring HCCH torsion	964	827	137	956	8
ring CH wag/$C^{\gamma}C^{\beta}$ wag	857	760	97	844	13
ring CH wag/O1C′O2 bend/ring torsion	781	740	41	773	8
C^{β}-ring wag/CH wag	600	557	43	541	59
($C^{\epsilon 1}C^{\gamma}C^{\epsilon 2}$/$C^{\delta 1}C^{\zeta}C^{\delta 2}$) out-of-plane bend/ring (CH+$C^{\zeta}O^{\eta}$) wag	481	423	58	471	10
$C^{\alpha}C^{\beta}C^{\gamma}$ bend/NH_2 rock	158	154	4	155	3
CH str	3152	2333	819	3142	10
CH str	3121	2306	815	3111	10
ring CC str/CH bend	1509	1470	39	1457	52
ring CC str	1466	1439	27	1416	50
ring CC str/$C^{\beta}H_2$ twist/$C^{\alpha}H$ wag	1350	1289	61	1320	30
ring CH bend/CC str/$C^{\beta}H_2$ twist	1247	997	250	1224	23
($C^{\beta}H_2$)C^{γ} rock/NH_2 wag	906	862	44	904	2
ring CH bend	1076	791	285	1068	8
CCC in-plane bend	608	585	23	586	22
$C^{\zeta}O^{\eta}$ bend/$C^{\beta}H_2$ rock	434	405	29	426	8

the peptide chain. These CH bending and out-of-plane ring bending modes are expected to be most sensitive to TyrO• conformation and are therefore most likely to show differences between our calculated frequencies and frequencies determined experimentally for TyrO• in proteins. They are therefore very important because they offer the greatest opportunity for detecting subtle conformational differences between TyrO• in different proteins. These calculations have not yet been performed because of the major investment of computer resources required. In addition, we do not report vibrational frequencies for modes concentrated on the peptide chain because the calculated gas-phase structure, with its CO_2H and NH_2 groups, differs from peptide chains in proteins and from zwitterionic TyrO• in water at neutral pH.

Frequency shifts for two different isotopically substituted TyrO• radicals have also been calculated to assist in mode assignments for the experimentally studied, isotopically substituted TyrO• from photosystem II.[32] Table 5 displays calculated frequencies and frequency shifts for TyrO• with deuterium replacing hydrogens on C^{α}, C^{β}, and the phenoxyl ring (TyrO•-d_7) and with ^{13}C enrichment at all positions of the phenoxyl ring (TyrO•-$^{13}C_6$). The largest frequency shifts calculated for modes concentrated on the phenoxyl ring of TyrO•-d_7 involve CH stretches and range from 809 to 819 cm^{-1}. Several modes that have already been observed experimentally for TyrO• also show calculated frequency shifts larger than 100 cm^{-1} in TyrO•-d_7, including the CH bending/CC stretching mode at 1418 cm^{-1} for TyrO• and 1186 cm^{-1} for TyrO•-d_7, the ring CH bending mode at 1139 cm^{-1} for TyrO• and 815 cm^{-1} for TyrO•-d_7, and the CCC trigonal bend at 970 cm^{-1} for TyrO• and 862 cm^{-1} for TyrO•-d_7. Other experimentally observed modes of TyrO• show smaller frequency shifts, ranging from 11 to 49 cm^{-1}, whereas large shifts of more than 100 cm^{-1} are calculated for five other modes. For TyrO•-$^{13}C_6$, calculated frequency shifts are generally much smaller than those calculated for TyrO•-d_7, but relatively large shifts are apparent in modes already experimentally detected for TyrO•. For example, the CC stretch (mode 8a) shifts by 56 cm^{-1}, the $C^{\zeta}O^{\eta}$ stretch shifts by 41 cm^{-1}, the CH bend/CC stretch moves 29 cm^{-1}, the CCC trigonal bend moves 26 cm^{-1}, and the ring breathing/CC stretching mode shifts 20 cm^{-1} lower in frequency. Large frequency shifts of more than 50 cm^{-1} are also calculated for three other modes of TyrO•-$^{13}C_6$. Since frequency shifts are naturally smaller in magnitude than absolute frequencies, our calculated frequency shifts should display less error than the frequencies themselves. Thus, the relative magnitudes of calculated isotopic frequency shifts should prove very useful in assigning vibrational frequencies already observed for TyrO• and for the isotopically substituted TyrO•-d_7 and TyrO•-$^{13}C_6$ radicals in PSII.

Unfortunately, very few band assignments are currently published for TyrO• in PSII.[32,103] Bands observed at 1480 cm^{-1}, and 1472 or 1504 cm^{-1} were assigned to the $C^{\zeta}O^{\eta}$ stretching mode and bands near 1550 and 1512 cm^{-1} were identified as candidates for the CC stretching mode[32] observed at 1565 cm^{-1} for *in vitro* TyrO•. Although the limited accuracy of our calculated frequencies, as well as possible contacts between TyrO• and neighboring water molecules or amino acid residues in proteins, makes it risky to identify experimental bands with calculated frequencies, some correlations and suggestions are possible. First, $^{18}O^{\eta}$ or $^{13}C^{\zeta}$ isotopic substitution gives calculated frequency shifts for the 7a $C^{\zeta}O^{\eta}$ stretching mode of −24 and −37 cm^{-1}, respectively. The only other modes with frequency shifts greater than 5 cm^{-1} are the Wilson modes 14 (1350 cm^{-1} for TyrO•, 1349 cm^{-1} for TyrO•-$^{18}O^{\eta}$, and 1339 cm^{-1} for TyrO•-$^{13}C^{\zeta}$) and 3 (1247 cm^{-1} for TyrO•, 1246 cm^{-1} for TyrO•-$^{18}O^{\eta}$, and 1227 cm^{-1} for TyrO•-$^{13}C^{\zeta}$). Thus, the $C^{\zeta}O^{\eta}$ stretching mode should represent the only band displaying a substantial isotopic frequency shift upon $^{18}O^{\eta}$ or $^{13}C^{\zeta}$ isotopic substitution and appearing in the frequency range above 1350 cm^{-1}. Second, the frequency difference between the CC stretching mode 8a and the $C^{\zeta}O^{\eta}$ stretching mode 7a is approximately constant: our calculated frequency difference is 56 cm^{-1} for TyrO• and 55 cm^{-1} for PhO•, whereas experimentally observed differences are 47 cm^{-1} for PhO•[36-38] and 55 cm^{-1} for TyrO• *in vitro*.[30]

Assuming no substantial non-covalent interactions to shift vibrational frequencies in the protein, the 8a mode should appear approximately 50 cm^{-1} higher than 7a. Finally, we must acknowledge that our SVWN density-functional calculations for TyrO• may misplace the 8b CC stretching mode relative to 7a. Our previous work for PhO• [45] demonstrates that all computational methods other than the SVWN method place 8b at a higher frequency than 7a. So, 8b may appear at a frequency between 8a and 7a for TyrO•. Resolving this question computationally will require more sophisticated calculations for TyrO•.

Conclusions

Density-functional quantum chemical calculations have been described to illustrate the similarities and differences in calculated structures, electronic spin densities, vibrational frequencies, and vibrational modes for phenoxyl (PhO•) and tyrosine phenoxyl (TyrO•) radicals. First, calculated bond distances between non-hydrogen atoms within the phenoxyl radical side chain of TyrO• differ from calculated bond distances for PhO• by an average of only 0.003 Å and a maximum of 0.009 Å. Both radicals display substantial C=O double bond character and, except for the two carbon−carbon bonds most distant from the phenoxyl oxygen, carbon−carbon distances are intermediate between distances observed for the corresponding bonds of phenol and *p*-benzoquinone. The two carbon−carbon bonds farthest from the phenoxyl oxygen, on the other hand, differ from those of phenol by only 0.004 Å. The striking structural similarity between the two radicals appears despite the proximity of the CO_2H and NH_2 groups located gauche to the phenoxyl side chain of TyrO• in the amino acid radical's most stable conformation (see **4a**). Next, calculated ratios of electronic spin densities on the atoms of PhO• and TyrO• agree well with experimentally derived spin density ratios. Calculated spin densities for the two radicals differ from each other by less than 0.03 and imply that the unpaired electron of TyrO• in its calculated, lowest-energy conformation resides entirely on its phenoxyl side chain. Both radicals thus display spin density distributions characteristic of odd-alternant hydrocarbons and qualitatively consistent with the magnitudes of atomic orbital coefficients for the singly occupied MO of PhO•.

Calculated vibrational frequencies for both PhO• and TyrO• agree well with experimentally determined frequencies and most vibrational frequencies and modes involving motions within the ring plane of PhO• and TyrO• are very similar to each other. The frequencies of TyrO• closest to those of PhO• include a number of experimentally observed, A_1 symmetry modes such as the highest frequency carbon−carbon stretch (Wilson mode 8a), the carbon−oxygen stretch (7a), a mixed CH bend/CC stretch (19a), and a CCC trigonal bending mode (mode 12). Calculated frequencies of these four modes are higher by only 7−16 cm^{-1} in TyrO• than in PhO•.

The modes which experience the largest frequency shift upon replacing the hydrogen of PhO• with the peptide chain of TyrO• are also identified. They include modes predominantly composed of $C^{\gamma}H^{\gamma}$ stretching, $C^{\gamma}H$ bending, ring breathing/CH bending, and $C^{\delta 1}C^{\gamma}C^{\delta 2}$ out-of-plane bending/CO wagging. The different bonding and mass of the peptide chain of TyrO• compared to the hydrogen it replaces in PhO• appears predominantly responsible for the largest calculated frequency shifts of 1830 cm^{-1} for the CH stretch ($C^{\gamma}C^{\beta}$ stretch for TyrO•) and 239 cm^{-1} for the CH bend (with substantial $C^{\gamma}C^{\beta}$ bending character in TyrO•). Interactions between the TyrO• C^{β} and adjacent ring hydrogens also appear to result in mixing of phenoxyl ring modes with motions of the peptide chain and yield substantial frequency shifts of 184 cm^{-1} for the PhO• ring breathing mode and 92 cm^{-1} for a CCC bending mode. These modes which display the largest mixing between the TyrO• peptide chain and phenoxyl side-chain motions are important because they offer the potential to detect conformational differences between TyrO• in different proteins.

Isotopic frequency shifts for TyrO• were also calculated to aid in mode assignments. Among the modes of TyrO• already observed experimentally, modes of TyrO•-d_7 displaying the largest isotopic frequency shifts include the CH bend/CC stretch (mode 19a; −232 cm^{-1} frequency shift), the ring CH bend (mode 9a; −324 cm^{-1} shift), and the CCC trigonal bend (mode 12; −108 cm^{-1} frequency shift). Experimentally observed modes of TyrO• that decrease the most for TyrO•-$^{13}C_6$ and their calculated frequency shifts, on the other hand, are the CC stretch (mode 8a; −56 cm^{-1}) and the $C^{\xi}O^{\eta}$ stretch (7a; −41 cm^{-1}). The CH bending/CC stretching (19a; −29 cm^{-1}), the CCC trigonal bending (12; −26 cm^{-1}), and the ring breathing/$C^{\alpha}C$ stretching modes (mode 1; −20 cm^{-1}) display smaller, but substantial frequency shifts for TyrO•-$^{13}C_6$. The $C^{\xi}O^{\eta}$ stretching mode 7a of TyrO• is also the only mode calculated to appear above 1350 cm^{-1} that shows a substantial frequency shift upon $^{18}O^{\eta}$ (−24 cm^{-1}) or $^{13}C^{\xi}$ (−37 cm^{-1}) isotopic substitution. These latter results suggest that the $^{18}O^{\eta}$ or $^{13}C^{\xi}$ isotopic substitution should offer a fine opportunity to identify unambiguously the $C^{\xi}O^{\eta}$ stretching mode 7a of TyrO• in proteins.

Acknowledgment. This work was supported by Grant No. 09180-01 from the National Institutes of Health, award No. CHE-9419734 from the National Science Foundation, and the University of Oklahoma Research Council through a Research Investment Grant and a Junior Faculty Research Fellowship. We are also grateful to the University of Oklahoma's University Computing Services and the Cornell Theory Center for providing computer time. The Cornell Theory Center receives major funding from the National Science Foundation and New York State. Additional funding comes from the Advanced Research Projects Agency, the National Institutes of Health, IBM Corporation, and other members of the center's Corporate Research Institute. R.W. also thanks Professor B. A. Barry, Dr. C. Berthomieu, and Dr. R. Hienerwadel for helpful discussions and Dr. C. Berthomieu for providing results prior to publication.

JA943578F